

Diffuse X-Ray Emission from the Quiescent Superbubble M 17, the Omega Nebula

Bryan C. Dunne¹, You-Hua Chu¹, C.-H. Rosie Chen¹, Justin D. Lowry¹, Leisa Townsley²,
Robert A. Gruendl¹, Martín A. Guerrero¹, and Margarita Rosado³

carolan@astro.uiuc.edu

ABSTRACT

The emission nebula M 17 contains a young ~ 1 Myr-old open cluster; the winds from the OB stars of this cluster have blown a superbubble around the cluster. *ROSAT* observations of M 17 detected diffuse X-ray emission peaking at the cluster and filling the superbubble interior. The young age of the cluster suggests that no supernovae have yet occurred in M 17; therefore, it provides a rare opportunity to study hot gas energized solely by shocked stellar winds in a quiescent superbubble. We have analyzed the diffuse X-ray emission from M 17, and compared the observed X-ray luminosity of $\sim 2.5 \times 10^{33}$ ergs s⁻¹ and the hot gas temperature of $\sim 8.5 \times 10^6$ K and mass of $\sim 1 M_{\odot}$ to model predictions. We find that bubble models with heat conduction overpredict the X-ray luminosity by two orders of magnitude; the strong magnetic fields in M 17, as measured from H I Zeeman observations, have most likely inhibited heat conduction and associated mass evaporation. Bubble models without heat conduction can explain the X-ray properties of M 17, but only if cold nebular gas can be dynamically mixed into the hot bubble interior and the stellar winds are clumpy with mass-loss rates reduced by a factor of ≥ 3 . Future models of the M 17 superbubble must take into account the large-scale density gradient, small-scale clumpiness, and strong magnetic field in the ambient interstellar medium.

Subject headings: ISM: bubbles — HII regions — ISM: individual (M17) — stars: early-type — stars: winds, outflows

¹Department of Astronomy, University of Illinois, 1002 West Green Street, Urbana, IL 61801

²Department of Astronomy & Astrophysics, Pennsylvania State University, 525 Davey Laboratory, University Park, PA 16802

³Instituto de Astronomía, Universidad Nacional Autónoma de México, Apdo. Postal 70-264, 04510 México, D.F., México

1. Introduction

Massive stars dynamically interact with the ambient interstellar medium (ISM) via their fast stellar winds and supernova ejecta. OB associations, with their large concentrations of massive stars, provide an excellent laboratory to study these interactions. The combined actions of the stellar winds and the supernovae from the massive stars in OB associations sweep up the ambient ISM to form expanding shells called superbubbles (Bruhweiler et al. 1980). The physical structure of a superbubble is very similar to that of a bubble blown by the stellar wind of an isolated massive star, as modeled by Castor, McCray, & Weaver (1975) and Weaver et al. (1977).

Theoretically, an interstellar bubble consists of a shell of swept-up ISM with its interior filled by shocked fast wind at temperatures of 10^6 – 10^8 K. There are two basic types of models for wind-blown bubbles: energy-conserving and momentum-conserving. In the former, the shocked stellar wind is separated from the swept-up interstellar shell by a contact discontinuity, where heat conduction and mass evaporation may take place. The expansion of the shell is driven by the pressure of the hot interior gas (Dyson & de Vries 1972; Castor et al. 1975). In the momentum conserving bubbles, the fast stellar winds impinge on the swept-up shell directly, and the expansion is driven by the momentum of the fast stellar wind (Avedisova 1972; Steigman, Strittmatter, & Williams 1975).

One significant difference between a superbubble and a single star bubble is the possibility that supernovae may occur inside a superbubble and introduce significant perturbations in the surface brightness and characteristic temperature of the X-ray emission, especially if a supernova explodes near the dense shell (Mac Low & McCray 1988). This intermittent X-ray brightening has been observed in superbubbles in the Large Magellanic Cloud (LMC). Using *Einstein* and *ROSAT* observations, Chu & Mac Low (1990) and Dunne, Points, & Chu (2001) have reported diffuse X-ray emission from a large number of superbubbles in the LMC, and their X-ray luminosities all exceed the luminosities expected by Weaver et al.’s bubble model, indicating recent heating by supernovae. No LMC superbubbles in a quiescent state, i.e., without recent supernova heating, have been detected in X-rays by *ROSAT* (Chu et al. 1995). It would be of great interest to detect diffuse X-ray emission from a quiescent superbubble and compare it to model expectations, as this could provide a valuable diagnostic of bubble models.

The emission nebula M17 (from the catalog of Messier 1850, $\alpha = 18^{\text{h}}21^{\text{m}}$, $\delta = -16^{\circ}10'$ (J2000.0), also known as the Omega Nebula, the Horseshoe Nebula, and NGC 6618) is located on the eastern edge of a massive molecular cloud, M17SW (Lada, Dickinson, & Penfield 1974). M17 exhibits a “blister-like” structure with an overall diameter of $\sim 20'$ – $25'$, or ~ 10 – 12 pc at an adopted distance of 1.6 kpc (Nielbock et al. 2001). The nebula encompasses

an open cluster with a stellar age of ~ 1 Myr (Hanson, Howarth, & Conti 1997). The open cluster is located on the western side of the nebula, which borders the molecular cloud. Arcuate filaments extend eastward, creating a shell morphology, and suggesting that it is a young superbubble blown by the OB stars within. The young age of the cluster in M17 implies that no supernova explosions have occurred, thus M17 provides an ideal setting to study the generation of hot gas solely by fast stellar winds inside a superbubble at a quiescent state.

Recent *Chandra* observations of M17 have revealed diffuse X-ray emission in the vicinity of the embedded open cluster (Townsend et al. 2003). As a matter of fact, diffuse X-ray emission from M17 over a more extended area was previously detected in a *ROSAT* observation but was never reported. We have analyzed this diffuse X-ray emission from the interior of M17 detected by *ROSAT* to determine the physical properties of the hot interior gas, and considered bubble models with and without heat conduction. We find that models with heat conduction produce results with the largest discrepancy from the observed X-ray luminosity and hot gas temperature and mass of the superbubble in M17. This paper reports our analysis of the *ROSAT* observations of M17 and comparisons to a range of bubble models.

2. Observations and Data Reduction

2.1. *ROSAT* Archival Data

We have used an archival *ROSAT* Position Sensitive Proportional Counter (PSPC) observation to study the diffuse X-ray emission from M17 and investigate the physical properties of the hot, shocked gas interior to the superbubble. The PSPC is sensitive to X-rays in the energy range 0.1–2.4 keV and has an energy resolution of $\sim 40\%$ at 1 keV, with a field of view of $\sim 2^\circ$. Further information on the PSPC can be found in the *ROSAT* Mission Description (1991).

The PSPC observation of M17 (sequence number RP500311, PI: Aschenbach) was obtained on 1993 September 12–13. It is centered on the nebula at $\alpha(\text{J2000}) = 18^{\text{h}} 21^{\text{m}} 04^{\text{s}}.78$ and $\delta(\text{J2000}) = -16^\circ 10' 12''.0$, and has an exposure time of 6.7 ks. As M17 has an angular size of $\sim 20' - 25'$, the diffuse X-ray emission from the superbubble interior is well contained within the inner window support ring of the PSPC. The PSPC data were reduced using standard routines in the PROS⁴ package under the IRAF⁵ environment.

⁴PROS/XRAY Data Analysis System – <http://hea-www.harvard.edu/PROS/pros.html>

⁵Image Reduction and Analysis Facility – IRAF is distributed by the National Optical Astronomy Ob-

2.2. Optical Imaging

To compare the spatial distribution of the X-ray-emitting gas with that of the cooler ionized gas in M17, we have obtained narrow-band $H\alpha$ images of this emission nebula. M17 was observed with the Mount Laguna 1-m telescope on 2002 October 28–31 using a Tektronik 2K CCD. A filter with peak transmission at 6563 \AA and a FWHM of 20 \AA was used to isolate the $H\alpha$ line. Because the 2K CCD has ~ 0.4 pixels and a field-of-view of $13.6'$, the entire nebula could not be observed in a single exposure. Instead a total of twenty-four 300 s exposures were acquired at 8 positions to span the nebula. These exposures were combined to form a mosaic image of the nebula and to reject cosmic-ray events in the individual images using the methods outlined in Regan & Gruendl (1995).

3. Analysis of the X-Ray Emission

Significant X-ray emission is detected from M17 in the PSPC observation, as can be seen in Figure 1. To determine the nature and origin of this emission, we have analyzed its spatial distribution and spectral properties. We have examined the distribution of the X-ray emission and compared it to the optical morphology of the emission nebula. We have also extracted spectra from the PSPC data and modeled them to determine the physical conditions of the hot gas.

3.1. Spatial Distribution of the X-ray Emission

To study the spatial distribution of the X-ray emission from M17, the data were binned to $5''$ pixels and then smoothed with a Gaussian function of $\sigma = 4$ pixels (see Figure 1a). We have also taken our $H\alpha$ mosaic and overlaid it with X-ray emission contours to study the extent of X-ray emission within the H II region (see Figure 1b). Diffuse X-ray emission is observed to be well confined by the optical nebula. This diffuse emission shows no evidence of limb brightening, suggesting that the interior of M17 is centrally filled with hot gas. The peak of the X-ray emission is coincident with the center of the open cluster in M17, where *Chandra* observations show a large number of point sources superposed on the diffuse emission (Townsend et al. 2003). This spatial distribution suggests that the X-ray-emitting hot gas originates in the open cluster, as would be expected in a bubble blown by stellar

winds. As there is a massive molecular cloud to the west of M17, we expect the hot gas to expand more rapidly to the east; this flow of hot gas to the east has then blown the blister-like bubble seen in optical images.

Four additional point sources are detected in the field around M17. The brightest of these point sources lies to the south of the X-ray peak and has been previously designated 1WGA J1820.6–1615 in the WGA Catalog of *ROSAT* Point Sources (White, Giommi, & Angelini 1994). This point source is coincident with OI 352 (Ogura & Ishida 1976), an O8 star on the southern edge of the open cluster in M17. The other three point sources lie on the northern edge of the emission nebula. These X-ray point sources, designated as 1WGA J1820.8–1603, 1WGA J1821.0–1600, and 1WGA J1820.8–1556, are coincident with stars GSC⁶ 06265–01977, SAO 161369 (a known O5 star), and GSC 06265–01808, respectively. These point sources are marked in Figure 1a.

3.2. X-Ray Spectra

In order to examine the spectra of the diffuse X-ray emission, we first excluded the point sources found in §3.1. Then, noting that M17 is on the edge of a dense molecular cloud, we have sectioned the nebula into four regions to account for anticipated changes in the foreground absorption column density. These regions have been labeled A, B, C, and D and are displayed in Figure 2. Additionally, we have selected a background annulus around the superbubble, as indicated in Figure 2. The background-subtracted spectra were then extracted from the PSPC event files.

The observed X-ray spectra of the superbubble is a convolution of several factors: the intrinsic X-ray spectrum of the superbubble, the intervening interstellar absorption, and the PSPC response function. Because the interstellar absorption and the PSPC response function are dependent on photon energy, we must assume models of the intrinsic X-ray spectrum and the interstellar absorption to make the problem tractable. As the X-ray emission from the superbubble interior appears largely diffuse, we have used the Raymond & Smith (1977) thermal plasma emission model to describe the intrinsic X-ray spectra of the superbubble and the Morrison & McCammon (1983) effective absorption cross-section per hydrogen atom for the foreground absorption, assuming solar abundances for both the emitting and absorbing materials. We then simulated the observed spectrum, combining the

⁶The Guide Star Catalog-I was produced at the Space Telescope Science Institute under U.S. Government grant. These data are based on photographic data obtained using the Oschin Schmidt Telescope on Palomar Mountain and the UK Schmidt Telescope.

assumed models for the intrinsic spectrum and the interstellar absorption with the response function of the PSPC. The best-fit spectrum is found by varying parameters and comparing χ^2 for the simulated and observed spectra.

We performed a χ^2 grid search of simulated spectral fits to determine the best-fit levels for the thermal plasma temperature, kT , and absorption column density, N_{H} . Plots of the best fits to the X-ray spectra are shown in Figure 3, and χ^2 plots are presented in Figure 4. The χ^2 plots of regions A, B, and C indicate that the X-ray emission can be fit by either higher temperature plasma, ~ 0.7 keV, with lower absorption column density, $\sim 10^{20-21}$ cm $^{-2}$, or lower temperature plasma, ~ 0.2 keV, with higher absorption column density, $\sim 10^{22}$ cm $^{-2}$. This is a common problem for PSPC spectra with a limited number of counts because of the poor spectral resolution and soft energy coverage of the PSPC. The best model fits favor the higher temperature plasma and lower absorption column density solution. Indeed, the detection of soft X-ray emission below 0.5 keV indicates that the solution with $N_{\text{H}} \sim 10^{22}$ cm $^{-2}$ cannot be valid, as such a solution predicts no significant soft X-ray emission should be detected. Furthermore, the high absorption column density solution predicts a foreground absorption column density for M17 equal to the total Galactic H I column density along the line of sight (Dickey & Lockman 1990). As M17 is located in the plane of the Galaxy at $l = 15^\circ 03'$, $b = -00^\circ 40'$ and has a distance of 1.6 kpc, we do not expect the majority of the Galactic H I toward this direction to be located in front of the superbubble.

From the model fits, we calculated the unabsorbed X-ray flux, and therefore the X-ray luminosity, L_{X} , of the diffuse X-ray emission from each source region. The normalization factor, A , of the thermal plasma model is equal to $\int n_e n_p dV / 4\pi D^2$, where n_e and n_p are the electron and proton number densities, V is the volume of the superbubble, and D is the distance to the source. Assuming a He:H number ratio of 1:10 and that the X-ray emitting gas is completely ionized, we find $n_e \simeq 1.2n_p$, and that the volume emission measure can be expressed as $\langle n_e^2 \rangle fV$, where f is the volume filling factor. We have used the diameter of the superbubble, ~ 10 – 12 pc, as the depth of the X-ray emitting gas in each source region. We determined the volume, V , of each source region by multiplying the surface area of the region by the depth and a geometric correction factor of 2/3 (approximated by the volume ratio of a sphere to a cylinder). Taking the volume filling factor to be $f=0.5$, we then calculated rms n_e in each region. The best-fit values of kT , A , N_{H} , L_{X} and rms n_e are given in Table 1. Note that the model fit to region D did not converge because it contains a large number of unresolved stellar sources as well as diffuse emission; only approximate values for the X-ray luminosity and absorption column density are given. See Townsley et al. (2003) for a detailed analysis of the *Chandra* observations of region D.

Combining our results from each of the source regions, we find a total diffuse X-ray lu-

minosity of $\sim 2.5 \times 10^{33}$ ergs s $^{-1}$ in the *ROSAT* PSPC 0.1–2.4 keV band, a mean characteristic temperature of $kT \sim 0.72$ keV or $T \sim 8.5 \times 10^6$ K, a mean electron density of ~ 0.09 cm $^{-3}$, and a total hot gas mass of $\sim 1 M_{\odot}$. We have calculated the total thermal energy in hot, shocked wind component of the superbubble to be $E_{\text{th}} \sim 1 \times 10^{48}$ ergs with a cooling timescale of $t_T \sim 40$ Myr. Given the stellar age of the open cluster, ~ 1 Myr, we do not expect significant radiative cooling to have occurred. As a rough check, we multiply the current X-ray luminosity by the age of the cluster and find that the total energy radiated away by the X-ray emission is $\lesssim 10\%$ of the total thermal energy.

4. Discussion

4.1. Comparisons with Model Expectations

We now compare the observed physical properties of M 17 determined above to theoretical calculations from basic wind-blown bubble models. Although the M 17 superbubble is in an inhomogeneous ambient medium with a significant density gradient and the cluster is off-centered (a more complex scenario than is considered in basic bubble models), if the superbubble structure is indeed governed by the physical processes prescribed by these models, we expect the properties of the diffuse X-ray emission to agree with predictions within similar orders of magnitude. We first consider the wind-blown bubble model of Weaver et al. (1977) and will later consider a wind-blown bubble model without heat conduction.

4.1.1. A Bubble with Heat Conduction

In the Weaver et al. model, heat conduction and mass evaporation act across the boundary between the hot interior gas and the nebular shell to lower the temperature and raise the density of the bubble interior. The temperature and electron density profiles of such a bubble have been calculated by Weaver et al. (1977), and the X-ray luminosities of such bubbles can be determined using two methods outlined by Chu et al. (1995). In the first method, we derive the expected X-ray luminosity from the observed physical properties of the gas in the 10^4 K ionized shell of swept-up ISM. In the second method, we use the spectral types of massive stars in M 17 to estimate the combined mechanical luminosity of the stellar winds and then derive the expected X-ray luminosity. These two methods use independent input parameters and thus allow us to check the consistency of the pressure-driven bubble model in addition to comparing the expected and observed X-ray luminosities.

X-Ray Luminosity Method 1: The Ionized Shell

The expected X-ray luminosity in the *ROSAT* band of 0.1–2.4 keV for the Weaver et al. (1977) wind-blown bubble model has been given by Chu et al. (1995),

$$L_X = (8.2 \times 10^{27} \text{ ergs s}^{-1}) \xi I(\tau) n_0^{10/7} R_{\text{pc}}^{17/7} V_{\text{km/s}}^{16/7}, \quad (1)$$

where ξ is the metallicity relative to the solar value and in this case we assume a value of unity, $I(\tau)$ is a dimensionless integral of value ~ 2 , n_0 is the number density of the ambient medium in cm^{-3} , R_{pc} is the radius of the superbubble in pc, $V_{\text{km/s}}$ is the expansion velocity of the superbubble in units of km s^{-1} . The ambient density n_0 cannot be measured directly, but assuming that the ram pressure of the expanding shell is equal to the thermal pressure of the ionized superbubble shell, the relation between the ambient density and the density of the ionized shell is given by

$$n_0 = (9/7) n_i k T_i / (\mu_a V_{\text{exp}}^2), \quad (2)$$

where n_i is the electron number density in the ionized shell, $T_i \sim 10^4$ K is the electron temperature in the ionized shell, V_{exp} is the expansion velocity of the bubble, and $\mu_a = (14/11)m_{\text{H}}$ (Weaver et al. 1977; Chu & Mac Low 1990). Adopting a mean electron density of $n_i \sim 300 \text{ cm}^{-3}$ (Felli, Churchwell, & Massi 1984) and an observed $V_{\text{exp}} \sim 25 \text{ km s}^{-1}$ (Clayton et al. 1985), we calculated an ambient density of $n_0 \sim 40 \text{ cm}^{-3}$. Given the superbubble radius of 5–6 pc, we have determined an expected X-ray luminosity of $\sim 3 \times 10^{35} \text{ ergs s}^{-1}$.

X-Ray Luminosity Method 2: Wind Luminosity from OB Stars

We can also calculate the expected X-ray luminosity in an energy-conserving, wind-blown bubble by the following equation from Chu et al. (1995),

$$L_X = (1.1 \times 10^{35} \text{ ergs s}^{-1}) \xi I(\tau) L_{37}^{33/35} n_0^{17/35} t_{\text{Myr}}^{19/35}, \quad (3)$$

where L_{37} is the mechanical luminosity of the stellar winds in units of $10^{37} \text{ ergs s}^{-1}$, and t_{Myr} is the age of the bubble in Myr. To remain independent of Method 1, we do not use the value of n_0 determined for that method. Rather, we use the following relations between ambient density, radius, wind luminosity, bubble age, and expansion velocity,

$$n_0 = (1.3 \times 10^8 \text{ cm}^{-3}) L_{37}^3 t_{\text{Myr}}^3 R_{\text{pc}}^{-5}, \quad (4)$$

$$t_{\text{Myr}} = (0.59 \text{ Myr}) R_{\text{pc}} / V_{\text{km/s}}, \quad (5)$$

(Weaver et al. 1977; Chu et al. 1995). We again take the expansion velocity to be $\sim 25 \text{ km s}^{-1}$ (Clayton et al. 1985) and the radius to be 5–6 pc and derive a bubble age of $\sim 0.13 \text{ Myr}$.

To determine the wind luminosity of M17, we examined its massive stellar content. Hanson et al. (1997) identified nine O stars and four late-O/early-B stars in the open cluster. Using the spectral types of these massive stars, we have estimated their terminal stellar wind velocities, effective temperatures, and luminosities based on the stellar parameters given by Prinja, Barlow, & Howarth (1990) and Vacca, Garmany, & Shull (1996). We then calculated the mass-loss rates for the OB stars in M17 by utilizing the empirically derived relationship between effective temperature, luminosity, and mass-loss rate of de Jager, Nieuwenhuijzen, & van der Hucht (1988). Table 2 lists the detected OB stars, their spectral types as determined from optical and K-band observations, their terminal wind velocities V_∞ , stellar effective temperatures T_{eff} , stellar luminosities L , and their mass-loss rates \dot{M} . We calculated the total mechanical luminosity of the stellar winds,

$$L_w = \Sigma(1/2)\dot{M}V_\infty^2, \quad (6)$$

from the OB stars to be $\sim 1 \times 10^{37}$ ergs s^{-1} . As noted by Felli et al. (1984), the identified OB stars can approximately account for the ionization of the emission nebula; we therefore expect our calculated wind mechanical luminosity to be reasonably complete as well. Assuming a relatively constant mechanical luminosity, we find a total energy deposited by stellar winds of $\sim 4 \times 10^{49}$ ergs over the life of the bubble. In addition, this value of the wind mechanical luminosity gives an ambient density of $\sim 60 \text{ cm}^{-3}$ and an expected X-ray luminosity of $\sim 5 \times 10^{35}$ ergs s^{-1} . This X-ray luminosity value is consistent to within a factor of two with the value found by Method 1.

Although the two methods of determining the expected X-ray luminosity are consistent with each other, they do not agree with the X-ray luminosity derived from the PSPC observation. The observed X-ray luminosity is ~ 100 – 200 times lower than expected from Weaver et al.’s bubble model. It is possible that stellar winds are clumpy, as suggested by Moffat & Robert (1994), then the conventionally derived mass loss rates would be reduced by a factor of ≥ 3 . Even using the reduced mass loss rates, the expected X-ray luminosity is more than 40 times too high. The observed temperature, density, and surface brightness of the hot gas in M17 do not agree with the model expectations, either. The physical conditions of the shocked stellar winds in Weaver et al.’s model are heavily modified by heat conduction and the hot gas mass is dominated by the nebular mass evaporated across the interface. The predicted temperature is 5.0 – 5.6×10^6 K near the center and decreases outward, the predicted density is 0.2 – 0.4 cm^{-3} near the center and increases outward, and the X-ray surface brightness is expected to show limb-brightening. Compared with observed properties, the expected temperature is too low, density is too high, and the X-ray morphology is inconsistent. The disagreements between observations and model expectations suggest that heat conduction may not play a dominant role in determining the physical conditions inside this superbubble.

Heat conduction can be suppressed by the presence of magnetic fields (Soker 1994; Band & Liang 1988). The magnetic field strength in M17 has been measured via the H I Zeeman effect to be 100–550 μG , peaking near the interface between the H II region and the molecular cloud M17SW (Brogan et al. 1999). Assuming a comparable magnetic field strength in the swept-up 10^4 K shell, we find the Alfvén speed to be 10–60 km s^{-1} which is comparable to or much greater than the isothermal sound velocity of the 10^4 K gas, 10 km s^{-1} for H atoms. In addition, the magnetic field strength and isothermal sound velocity indicate a gyro-radius of $\lesssim 10$ km for protons in the swept-up shell. This suggests that the protons in the 10^4 K gas will be unable to escape the magnetic field and diffuse into the interior of the superbubble, inhibiting heat conduction and mass evaporation between the hot interior and the cool shell of the bubble.

4.1.2. A Bubble without Heat Conduction

We now turn our consideration to a wind-blown bubble without heat conduction. The X-ray emission of a bubble interior depends on both the temperature and the amount of hot gas. We will first compare the plasma temperature expected from the shocked stellar winds to the observed hot gas temperature. Using the combined stellar winds mass-loss rate of $4.3 \times 10^{-6} M_{\odot} \text{ yr}^{-1}$ (summed from Table 2) and the integrated wind mechanical luminosity L_w of $1 \times 10^{37} \text{ ergs s}^{-1}$ as calculated in §4.1.1, we derive an rms terminal wind velocity of $V_{\infty} \sim 2700 \text{ km s}^{-1}$. The post-shock temperature of the combined stellar winds is therefore expected to be $\sim 8 \times 10^7$ K. This temperature is an order of magnitude higher than that indicated by PSPC observations; to lower it to the observed temperature of $\sim 8.6 \times 10^6$ K requires the mixing in of cold nebular mass that is nearly 10 times the mass of the combined stellar winds. This mixing may be provided by turbulent instabilities at the interface between the shocked fast winds and the cold nebular shell (e.g., Strickland & Stevens 1998) or through the hydronamic ablation of clumps of cold nebular material distributed within the hot bubble interior (Pittard, Hartquist, & Dyson 2001).

Assuming that mixing has taken place, we next determine the hot gas mass expected as a result of mixing and compare it to the observed value (§3.2). Given the dynamical age of the superbubble, 0.13 Myr, a total stellar wind mass of $\sim 0.56 M_{\odot}$ has been injected to the superbubble interior, and the expected total mass of the hot gas will be 5–6 M_{\odot} . This is significantly greater than the observed value of $\sim 1 M_{\odot}$. This discrepancy can be reduced if we again consider the possibility of clumpy stellar winds (Moffat & Robert 1994). With the mass-loss rates reduced by a factor of ≥ 3 , the expected hot gas mass is $\sim 2 M_{\odot}$, which would be in remarkable agreement with the observed value.

We summarize the comparison between the observed X-ray emission and the various models in Table 3, which lists the observed X-ray luminosity and hot gas temperature and mass as well as those expected from models with and without heat conduction for both homogeneous winds and clumpy winds. It is clear that bubble models with heat conduction have the largest discrepancies from the observations. The best agreement with observed properties is from bubble models without heat conduction but allowing dynamical mixing of cold nebular material with the hot gas. For models either with or without heat conduction, clumpy winds with reduced mass loss rates are needed to minimize the discrepancy between model expectations and observations.

4.2. Comparisons with Other Wind-Blown Bubbles

Diffuse X-ray emission has been previously detected from other types of wind-blown bubbles, including planetary nebulae (PNe) and circumstellar bubbles blown by Wolf-Rayet (WR) stars. The X-ray emission from these circumstellar bubbles is qualitatively and quantitatively different from that of M17. Chu, Gruendl, & Guerrero (2003) find that the X-ray emission from PNe and WR bubbles shows a limb-brightened spatial distribution, in sharp contrast to the centrally-filled spatial distribution in M17 as described in §3.1. Further, Chu et al. (2003) note that PNe and WR bubbles exhibit hot gas temperatures of $1\text{--}3 \times 10^6$ K and electron densities of $10\text{--}100 \text{ cm}^{-3}$, while the hot interior gas of M17 exhibits a temperature of 8.5×10^6 K and a substantially lower electron density of $\sim 0.09 \text{ cm}^{-3}$.

The comparisons of morphology and temperature between the M17 superbubble and small circumstellar bubbles show fundamental differences. The limb-brightened X-ray spatial distribution, low temperatures, and high electron densities of PNe and WR bubbles are qualitatively consistent with a hypothesis of heat conduction and mass evaporation occurring between the hot gas interior and the swept-up shell. However, the observed X-ray luminosities for PNe and WR bubbles are both significantly lower (10–100 times) than predicted by bubble models with heat conduction (Chu et al. 2001; Wrigge, Wendker, & Wisotzki 1994; Wrigge 1999). It is possible that in these wind-blown bubbles, heat conduction has also been suppressed and that dynamical mixing, which allows a lower mass injection rate, occurs at the interface between the hot gas interior and the cool nebular shell. Exploring this question will require magnetic field measurements of PNe and WR bubbles.

5. Summary

We have presented analysis of a *ROSAT* observation of the emission nebula M17. The blister-like morphology seen in the optical images indicates that it is a superbubble blown by the winds of its OB stars in an inhomogeneous ISM. With a stellar age of ~ 1 Myr, M17 must be a young quiescent superbubble without any supernova heating. Diffuse X-ray emission is detected from M17 and is confined within the optical shell. This suggests the presence of hot 10^6 – 10^8 K gas in the interior of M17, as is expected in a wind-blown bubble. Analysis of the diffuse X-ray emission indicates a characteristic gas temperature $\sim 8.5 \times 10^6$ K with a mean electron number density of 0.09 cm^{-3} .

We have considered bubble models with and without heat conduction and found that those with heat conduction overpredict the X-ray luminosity by two orders of magnitude. Furthermore, the magnetic field measured in M17 is large enough to suppress heat conduction and associated mass evaporation. Bubble models without heat conduction overestimate the hot gas temperature unless mixing with cold nebular gas has occurred. If nebular gas can be dynamically mixed into the hot bubble interior and if the stellar winds are clumpy with a lower mass-loss rate, the X-ray morphology and luminosity, and hot gas temperature and mass can be reasonably reproduced.

M17 provides us a rare opportunity to probe the physical conditions of hot gas energized solely by shocked stellar winds in a quiescent superbubble. While we have learned much from the current analysis, our model considerations were performed on a very basic level. More robust models are needed to accurately describe the evolution of a superbubble in a medium with a large-scale density gradient, small-scale clumpiness, and a strong magnetic field.

We would like to thank the anonymous referee for the stimulating comments which have helped us to improve this paper. This research has made use of data obtained through the High Energy Astrophysics Science Archive Research Center Online Service, provided by the NASA/Goddard Space Flight Center.

REFERENCES

- Avedisova, V. S. 1972, *Soviet Astronomy*, 15, 708
- Band, D. L. & Liang, E. P. 1988, *ApJ*, 334, 266
- Brogan, C. L., Troland, T. H., Roberts, D. A., & Crutcher, R. M. 1999, *ApJ*, 515, 304
- Bruhweiler, F. C., Gull, T. R., Kafatos, M., & Sofia, S. 1980, *ApJ*, 238, L27
- Bumgardner, T. E. 1992, M.S. thesis, Ohio State Univ., Columbus (1992) , 2
- Castor, J., Weaver, R., & McCray, R. 1975, *ApJ*, 200, L107
- Chu, Y.-H. & Mac Low, M. 1990, *ApJ*, 365, 510
- Chu, Y.-H., Chang, H., Su, Y., & Mac Low, M. 1995, *ApJ*, 450, 157
- Chu, Y.-H., Gruendl, R. A., & Guerrero, M. A. 2003, *RevMexAA(SC)*, 15, 62
- Chu, Y., Guerrero, M. A., Gruendl, R. A., Williams, R. M., & Kaler, J. B. 2001, *ApJ*, 553, L69
- Clayton, C. A., Ivchenko, V. N., Meaburn, J., & Walsh, J. R. 1985, *MNRAS*, 216, 761
- Crampton, D., Georgelin, Y. M., & Georgelin, Y. P. 1978, *A&A*, 66, 1
- de Jager, C., Nieuwenhuijzen, H., & van der Hucht, K. A. 1988, *A&AS*, 72, 259
- Dickey, J. M. & Lockman, F. J. 1990, *ARA&A*, 28, 215
- Dunne, B. C., Points, S. D., & Chu, Y.-H. 2001, *ApJS*, 136, 119
- Dyson, J. E. & de Vries, J. 1972, *A&A*, 20, 223
- Felli, M., Churchwell, E., & Massi, M. 1984, *A&A*, 136, 53
- Hanson, M. M., Howarth, I. D., & Conti, P. S. 1997, *ApJ*, 489, 698
- Lada, C., Dickinson, D. F., & Penfield, H. 1974, *ApJ*, 189, L35
- Mac Low, M.-M., & McCray, R. 1988, *ApJ*, 324, 776
- Messier, C. 1850, *Connaissance des Temps*, 1784, 227
- Moffat, A. F. J., & Robert, C. 1994, *ApJ*, 421, 310

- Morrison, R., & McCammon, D. 1983, ApJ, 270, 119
- Nielbock, M., Chini, R., Jütte, M., & Manthey, E. 2001, A&A, 377, 273
- Ogura, K. & Ishida, K. 1976, PASJ, 28, 35
- Pittard, J. M., Hartquist, T. W., & Dyson, J. E. 2001, A&A, 373, 1043
- Prinja, R. K., Barlow, M. J., & Howarth, I. D. 1990, ApJ, 361, 607
- Raymond, J. C., & Smith, B. W. 1977, ApJS, 35, 419
- Regan, M. W. & Gruendl, R. A. 1995, in ADASS IV Proceedings, ASP Conference Series 77, eds. R. A. Shaw, H. E. Payne, & J. J. E. Hayes, 335
- ROSAT* Mission Description, 1991, NASA publication NRA 91-OSSA-25, Appendix F
- Soker, N. 1994, AJ, 107, 276
- Steigman, G., Strittmatter, P. A., & Williams, R. E. 1975, ApJ, 198, 575
- Strickland, D. K. & Stevens, I. R. 1998, MNRAS, 297, 747
- Townsley, L., Feigelson, E. D., Montmerle, T., Broos, P. S., Chu, Y.-H., & Garmire, G. P. 2003, submitted to ApJ
- Vacca, W. D., Garmany, C. D., & Shull, J. M. 1996, ApJ, 460, 914
- Weaver, R., McCray, R., Castor, J., Shapiro, P., & Moore, R. 1977, ApJ, 218, 377
- White, N. E., Giommi, P., & Angelini, L. 1994, IAU Circ., 6100, 1 (Also, URL: <http://wgacat.gsfc.nasa.gov/wgacat/>)
- Wrigge, M., Wendker, H. J., & Wisotzki, L. 1994, A&A, 286, 219
- Wrigge, M. 1999, A&A, 343, 599

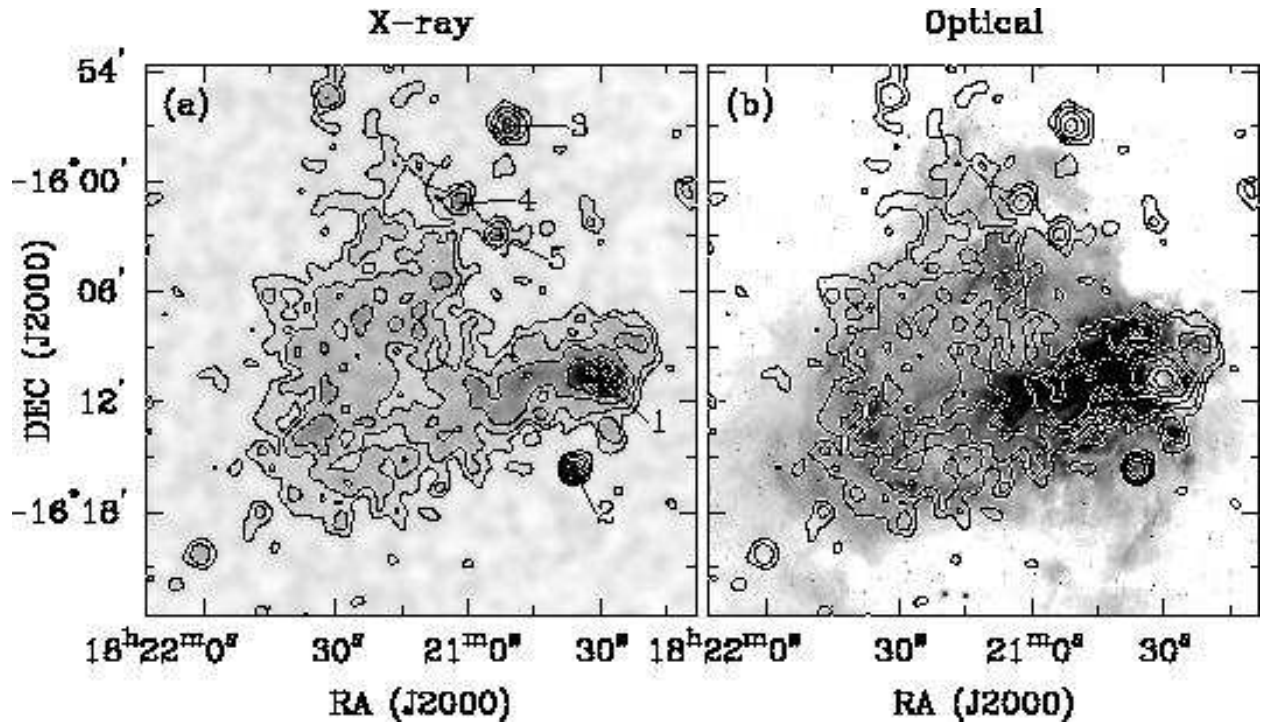


Fig. 1.— M17 in X-rays and optical. (a) shows a smoothed *ROSAT* PSPC X-ray image of M17; (b) shows M17 in H α emission overlaid with X-ray contours at 4.5%, 6.1%, 10%, 17%, 32%, and 61% of the peak value. These contours are also present on the X-ray image to ensure the clarity of the contours. Potential point sources are labeled on the X-ray image: (1) The OB association of M17, (2) 1WGA J1820.6–1615, (3) 1WGA J1820.8–1556, (4) 1WGA J1821.0–1600, and (5) 1WGA J1820.8–1602.

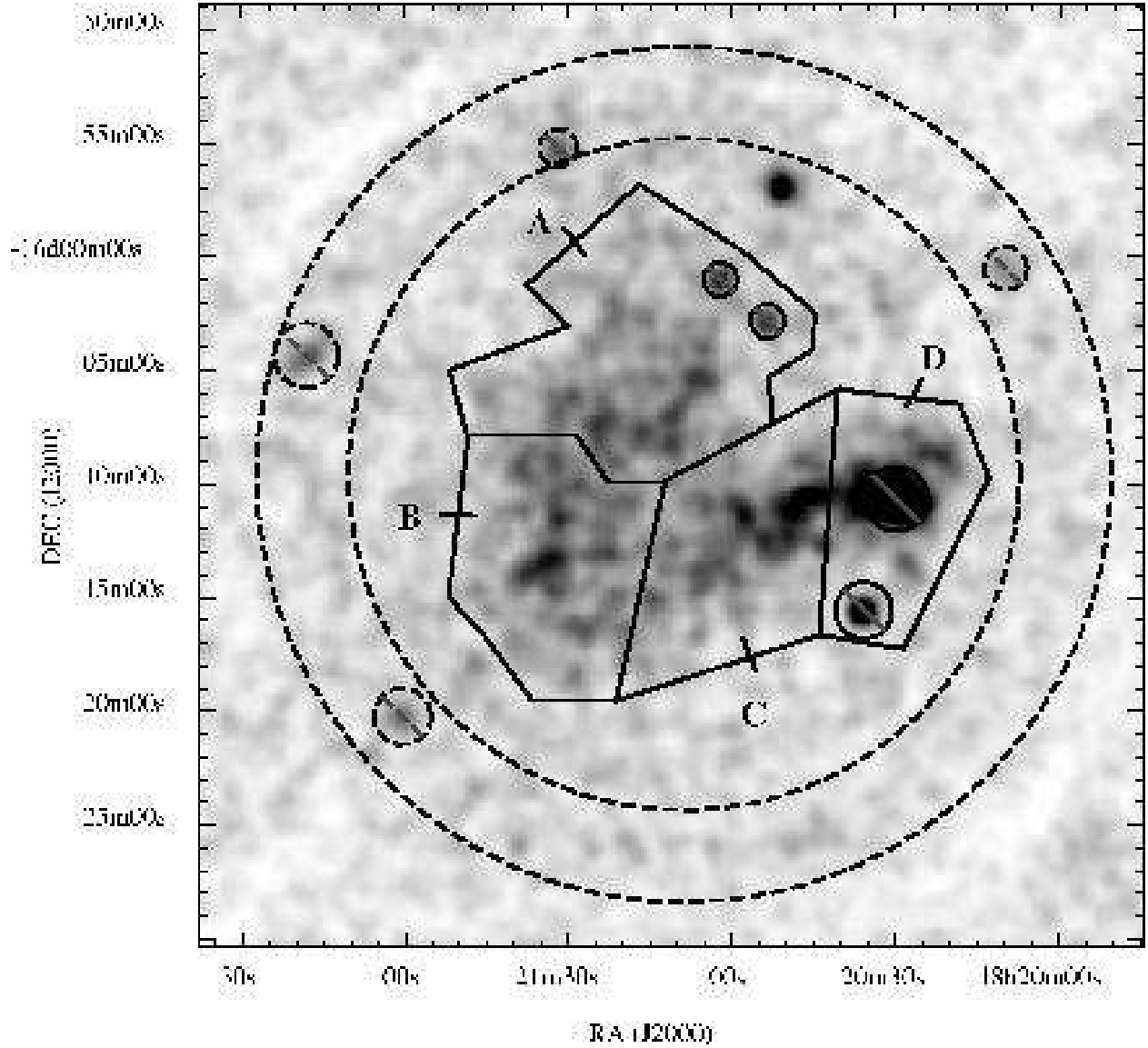


Fig. 2.— *ROSAT* PSPC X-ray emission image overlaid with the source regions used to extract and analyze the spectral properties of the diffuse X-ray emission. The source regions are A, B, C, and D. The region used for background subtracted is indicated by the dashed annulus. Potential point-sources excluded from the source and background regions are drawn as slashed circles.

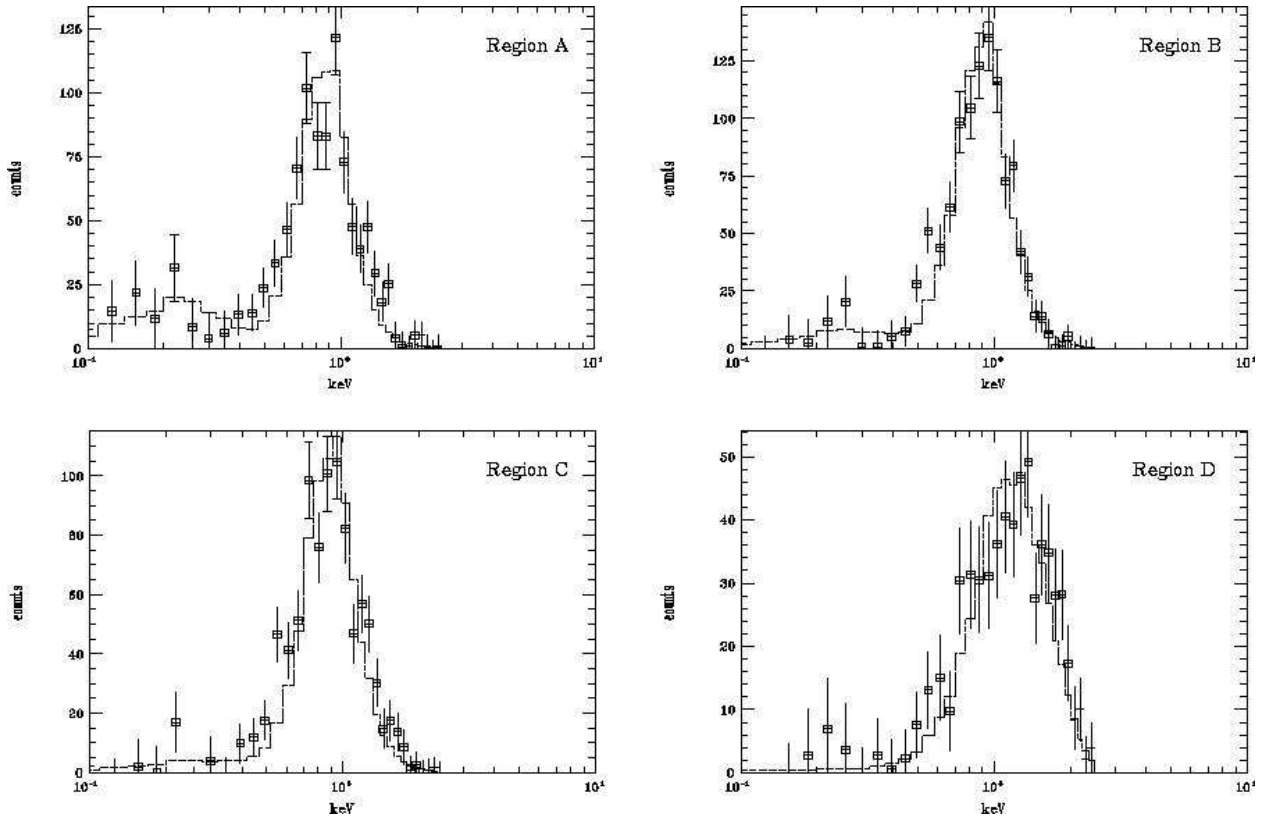


Fig. 3.— These *ROSAT* PSPC count plots show the X-ray spectrum extracted from each source region and the best thermal plasma model.

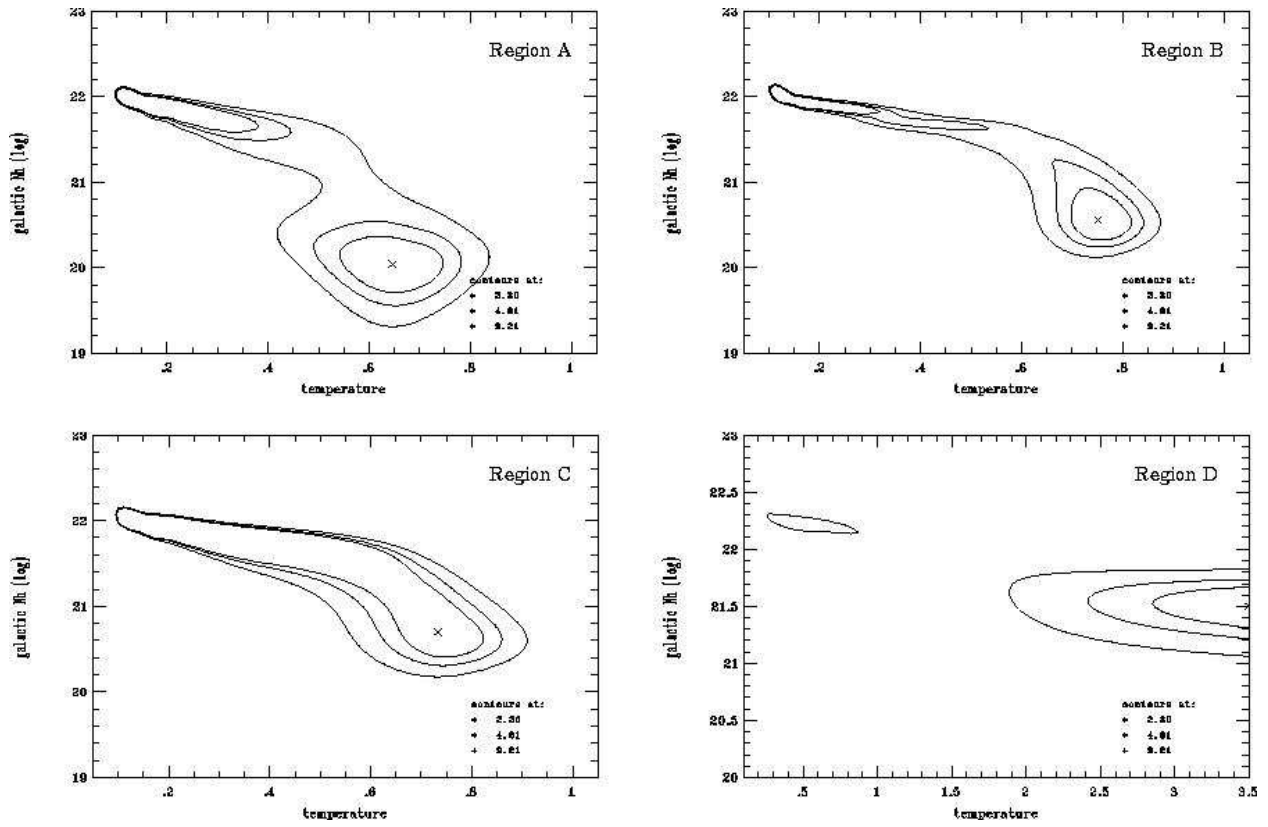


Fig. 4.— χ^2 plots for the X-ray spectral model fits to each source region. Confidence levels at 99%, 90%, and 68% are indicated as contours and the best fit location is marked with a \times .

Table 1: M 17 X-Ray Spectral Fits

Region	kT [keV]	A [cm ⁻⁵]	$\log N_{\text{H}}$ [cm ⁻²]	L_{X}^{a} [ergs s ⁻¹]	rms n_e [cm ⁻³]
A	0.65	4.3×10^{10}	20.04	4.4×10^{32}	6.5×10^{-2}
B	0.75	7.0×10^{10}	20.57	6.3×10^{32}	9.1×10^{-2}
C	0.73	5.3×10^{10}	20.70	5.2×10^{32}	9.3×10^{-2}
D ^b	–	–	21.5	1×10^{33}	–

^aIn the 0.1–2.4 keV energy band

^bFit did not converge, values approximated

Table 2: OB Stars in M 17 and their Stellar Wind Parameters

Star Number ^a	Optical Spectral Type ^b	K-Band Spectral Type ^b	V_{∞} ^d [km s ⁻¹]	T_{eff} ^e [K]	$\log L/L_{\odot}$ ^e	$\log \dot{M}$ ^f [M_{\odot} yr ⁻¹]
B98	O9V	kO9–B1	1500	36000	5.1	–6.8
B111	O5V	kO3–O4	2900	46000	5.7	–6.2
B137	...	kO3–O4	3100	50000	6.0	–6.0
B164	O7–O8V	kO7–O8	2000	40000	5.3	–6.6
B174	...	kO3–O6	2900	47000	5.8	–6.2
B181	...	kO9–B2	1500	33000	4.7	–7.2
B189	O5V	kO3–O4	2900	46000	5.7	–6.2
B243	early B	^c	500	22000	3.3	–11.1
B260	O7–O8V	kO3–O4	2000	40000	5.3	–6.6
B268	B2	^c	500	22000	3.3	–11.1
B289	O9.5V	^c	1500	35000	5.0	–6.9
B311	...	kO9–B2	1500	33000	4.7	–7.2
OI 345	O6V	kO5–O6	2600	44000	5.6	–6.4

^aFrom Bumgardner (1992), except OI 345 from Ogura & Ishida (1976)

^bFrom Hanson et al. (1997), except OI 345 from Crampton, Georgelin, & Georgelin (1978)

^cShows excess K-band emission, most likely a young stellar object.

^dAdopted from Prinja et al. (1990).

^eAdopted from Vacca et al. (1996).

^fFrom empirical relationship of de Jager et al. (1988).

Table 3: M 17 Observed and Model X-ray Properties

	L_X [10^{33} ergs s^{-1}]	Temperature [10^6 K]	Hot Gas Mass [M_\odot]
Observed	2.5	8.5	1
Model: Heat Conduction			
Method 1 ^a	3.1×10^2	5.0	$\gtrsim 4$
Method 2			
Homogeneous Winds ^a	5.2×10^2	5.6	$\gtrsim 9$
Clumpy Winds ^a	1.1×10^2	4.1	$\gtrsim 4$
Model: No Heat Conduction			
Without Dynamical Mixing			
Homogeneous Winds	0.2	80	0.5
Clumpy Winds	0.03	80	0.2
With Dynamical Mixing			
Homogeneous Winds	75	8.5	5–6
Clumpy Winds	10	8.5	2

^aCentral temperature as derived from the Weaver et al. (1977) model.